Solid-Solution Phosphors

International Edition: DOI: 10.1002/anie.201903178
German Edition: DOI: 10.1002/ange.201903178

Structural Evolution and Effect of the Neighboring Cation on the Photoluminescence of $Sr(LiAl_3)_{1-x}(SiMg_3)_xN_4:Eu^{2+}$ Phosphors

*Mu-Huai Fang, Sebastian Mahlik, Agata Lazarowska, Marek Grinberg, Maxim S. Molokeev, Hwo-Shuenn Sheu, Jyh-Fu Lee, and Ru-Shi Liu**

Abstract: *In this study, a series of $Sr(LiAl_3)_{1-x}(SiMg_3)_xN_4:Eu^{2+}$ (SLA-SSM) phosphors were synthesized by a solid-solution process. The emission peak maxima of SLA-SSM range from 615 nm to 680 nm, which indicates structural differences in these materials. ^{7}Li solid-state NMR spectroscopy was utilized to distinguish between the $Li(1)N_4$ and $Li(2)N_4$ tetrahedra in SLA-SSM. Differences in the coordination environments of the two Sr sites were found which explain the unexpected luminescent properties. Three discernible morphologies were detected by scanning electron microscopy. Temperature-dependent photoluminescence and decay times were used to understand the diverse environments of europium ions in the two strontium sites Sr1 and Sr2, which also support the NMR analysis. Moreover, X-ray absorption near-edge structure studies reveal that the Eu^{2+} concentration in SLA-SSM is much higher than that in in $SrLiAl_3N_4:Eu^{2+}$ and $SrSiMg_3N_4:Eu^{2+}$ phosphors. Finally, an overall mechanism was proposed to explain the how the change in photoluminescence is controlled by the size of the coordinated cation.*

High-quality lighting systems with high-color rendering index and high energy consumption efficiency are of great interest.[1–4] Among all lighting systems, light-emitting diodes (LEDs) stand out. Phosphor materials, which are used to tune the color of LEDs, must be explored urgently, especially for the red phosphor. In the past few years, a number of narrow-band-emission nitride phosphors have been developed.[5–15] Among the developed phosphors, $SrLiAl_3N_4:Eu^{2+}$ (SLA) is a promising phosphor for next-generation high-quality lighting.[16,17] It has an extremely narrow emission band ($\approx$50 nm) and excellent thermal stability. However, the emission wavelength at approximately 650 nm is slightly too long for SLA to serve as the red component in LED devices and would decrease the luminous efficacy of radiation (LER) due to the low sensitivity of the human eye to light of this wavelength.[18] Another well-designed nitride phosphor is $SrSiMg_3N_4:Eu^{2+}$ (SSM). Because of its single Sr site and ordered channel structure, its emission band is even narrower ($\approx$43 nm) than that of SLA. Moreover, its emission wavelength at approximately 610 nm is very short for the red component but can provide higher LER. The most serious disadvantage of SSM is its weak thermal stability due to the small band gap, causing serious thermal ionization.[6] The basic data for both are shown in Table S1. As a result, solid-solution methods may be a good was to combine the advantages of both phosphors and design the best materials by tuning the chemical composition.

In 2017, a series of UCr_4C_4-type solid-solution phosphors were prepared by Cui et al at normal pressure.[19] In their study, the solid solutions display emission ranging from 607 to 663 nm. Moreover, the thermal stability was analyzed by constructing host-referred binding energy (HRBE) and vacuum-referred binding energy (VRBE) schemes. However, in our study, we aim to understand the precise change of local structure in the solid solution $Sr(LiAl_3)_{1-x}(SiMg_3)_xN_4:Eu^{2+}$ (SLA-SSM), which was prepared under an atmosphere of 9 atm N_2, and its effect on the emission spectra.

In this study, $Sr(LiAl_3)_{1-x}(SiMg_3)_xN_4:Eu^{2+}$ (SLA-SSM) phosphors were synthesized. All as-prepared samples are consistent with expectation and were examined by X-ray diffraction (XRD). Part of their emission is out of the range from SLA (650 nm) to SSM (610 nm), which indicates the existence of unexpected structural change. Distinctively, the unknown region displays properties different from those of SLA and SSM in terms of photoluminescence, morphology, the oxidation state of Eu ion, and solid-state NMR signal. This study is expected to help the researcher understand the

[*] Dr. M. H. Fang, Prof. Dr. R. S. Liu
Department of Chemistry, National Taiwan University
Taipei 106 (Taiwan)
E-mail: rsliu@ntu.edu.tw
Prof. Dr. R. S. Liu
Department of Mechanical Engineering
and Graduate Institute of Manufacturing Technology
National Taipei University of Technology
Taipei 106 (Taiwan)
Dr. S. Mahlik, Dr. A. Lazarowska, Prof. Dr. M. Grinberg
Institute of Experimental Physics
Faculty of Mathematics, Physics and Informatics
Gdańsk University
Wita Stwosza 57, 80-308 Gdańsk (Poland)
Prof. M. S. Molokeev
Laboratory of Crystal Physics, Kirensky Institute of Physics
Federal Research Center KSC SB RAS
Krasnoyarsk 660036 (Russia)
and
Siberian Federal University
Krasnoyarsk 660041 (Russia)
and
Department of Physics, Far Eastern State Transport University
Khabarovsk 680021 (Russia)
Dr. H. S. Sheu, Dr. J. F. Lee
National Synchrotron Radiation Research Center
Hsinchu 300 (Taiwan)
Supporting information and the ORCID identification number(s) for the author(s) of this article can be found under: https://doi.org/10.1002/anie.201903178.

unexpected properties of solid solutions and provide an insight into the analysis methods.

XRD patterns were used to examine the phase of the solid-solution powders (Figure 1a). All phases are nearly pure except for some AlN impurities. With the doping of SLA with Mg and Si ions, the XRD peaks shift toward a lower angle, and no peak exists at around 37.1°, which proves the success of the solid-solution process. The crystal structures of SLA and SSM are quite similar to each other (Figure S1a,b). Both consist of tetrahedra with extremely high rigidity and ordering structure. SLA belongs to a triclinic system with the space group of $P\bar{1}$. Moreover, Li^+ and Al^{3+} ions form $[LiN_4]$ and $[AlN_4]$ tetrahedra. In contrast, SSM belongs to a tetragonal system with the space group of $I4_1/a$. Mg^{2+} and Si^{4+} form $[MgN_4]$ and $[SiN_4]$ tetrahedra, respectively. Two Sr sites exist in the SLA structure, whereas only one Sr site exists in the SSM structure. Eu ions will substitute in the Sr sites since the cations have a similar size of the cations and the same oxidation state. From the chemical formula, $Sr(LiAl_3)_{1-x}$-$(SiMg_3)_xN_4$:Eu^{2+}, Li^+ and Al^{3+} will be replaced by Si^{4+} and Mg^{2+}, respectively, due to the charge balance. Both XRD patterns are quite similar, but the alignment of the tetrahedra along the channel direction is different (Figure S1). If all Li^+ and Al^{3+} ions are replaced by Si^{4+} and Mg^{2+} ions, the solid solution cannot be formed.

To demonstrate the substitution process more clearly, the XRD contour plot for $Sr(LiAl_3)_{1-x}(SiMg_3)_xN_4$:$Eu^{2+}$ is shown in Figure S2. The peaks shift smoothly toward a lower angle except for some vertical lines, which belong to the AlN impurity. A break is noticeable at around 29° for $x = 0.6$–0.8, which may correspond to the phase transition from triclinic (SLA) to tetragonal (SSM) phase. The peak splitting at 29° for $x = 0.7$ also proves this assumption, as shown in the inset of Figure 1a. To further understand this property, we measured the synchrotron XRD and conducted Rietveld refinement, as shown in Figure S3 and Table S2. Comparable amounts of tetragonal phase ($I4_1/a$) and triclinic phase ($P\bar{1}$) are evident in $Sr(LiAl_3)_{0.2}(SiMg_3)_{0.8}N_4$:$Eu^{2+}$ (Figure 1b), which reveals the phase transition process. The volume of the unit cell refined from the synchrotron XRD data (Figure 1c) increases in accordance with the peak shift toward a lower angle.

The photoluminescence emission (PL) and excitation (PLE) spectra are shown in Figure 2a and Figure S4a, respectively. In the excitation spectra it is evident that

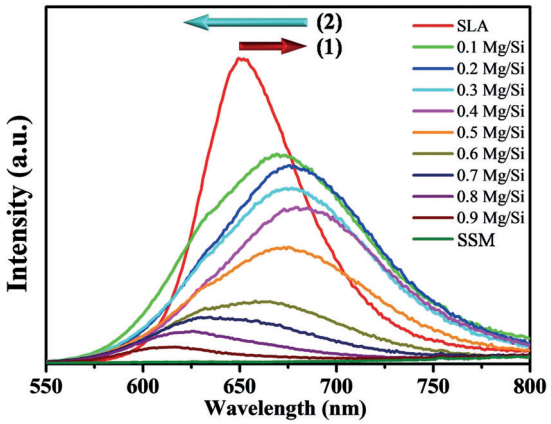

Figure 2. Photoluminescence spectra of $Sr(LiAl_3)_{1-x}(SiMg_3)_xN_4$:$Eu^{2+}$.

$Sr(LiAl_3)_{1-x}(SiMg_3)_xN_4$:$Eu^{2+}$ can be effectively excited by the 460 nm blue light. The normalized photoluminescence spectra are shown in Figure S4b. SLA displays 650 nm emission with a bandwidth of 50 nm. Interestingly, when Si^{4+} and Mg^{2+} are co-doped into SLA, the emission spectra for $Sr(LiAl_3)_{1-x}(SiMg_3)_xN_4$:$Eu^{2+}$ show a redshift until $x = 0.4$ (679 nm), which is even longer than the emission wavelength of SLA (650 nm); at higher x values the emission shifts toward shorter wavelengths. At $x = 0.1$ and $x = 0.2$, $Sr(LiAl_3)_{1-x}$-$(SiMg_3)_xN_4$:Eu^{2+} shows a larger integrated emission area than that of SLA itself, which indicates a potential chemical

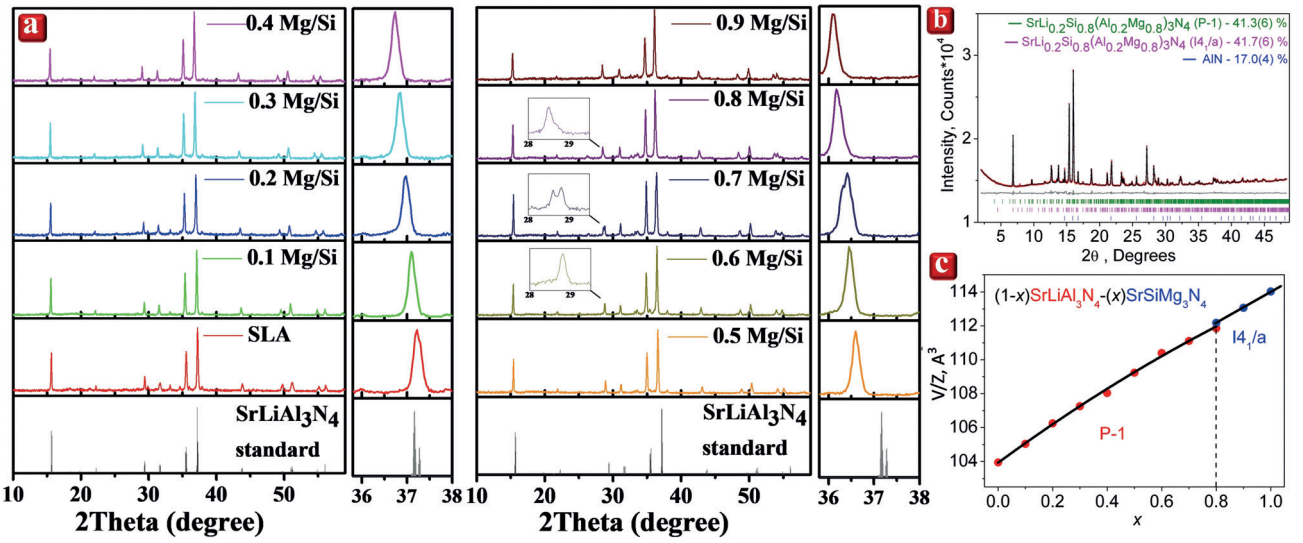

Figure 1. a) XRD patterns of $Sr(LiAl_3)_{1-x}(SiMg_3)_xN_4$:$Eu^{2+}$. b) XRD Rietveld refinement of $Sr(LiAl_3)_{0.2}(SiMg_3)_{0.8}N_4$:$Eu^{2+}$. c) Volume change of $Sr(LiAl_3)_{1-x}(SiMg_3)_xN_4$:$Eu^{2+}$.

composition for practical application. The details of the photoluminescence spectra are shown in Table S3. To quantify our findings, we measured internal quantum efficiency (IQE), absorption, and external quantum efficiency (EQE) as shown in Table S4. The EQE values for the samples with $x =$ 0.2–0.4 (EQE = 0.28–0.32) are higher than that for SLA (0.26).

The synthesis conditions are consistent for all the compounds, which means all the as-prepared samples are synthesized at temperatures under 1000 °C. However, in our experience, the best temperatures for SSM synthesis are around 1350 °C, which indicates potential room for improvement. Besides, during the incorporation of the Si/Mg ions, the emission full-width at half-maximum (fwhm) becomes much larger with the change of band shape from symmetric to asymmetric. This indicates that the two emission sites are very different from each other, which result in the broadening of the emission spectra. The incorporation process will also decrease the structure rigidity, which will also lead to the broadening of the PL spectra.

To further understand the luminescence properties of Eu^{2+} in the two Sr sites, Sr^{I} and Sr^{II}, the room-temperature PLE spectra of $Sr(LiAl_3)_{1-x}(SiMg_3)_xN_4:Eu^{2+}$ for $x = 0$, 0.1, 0.5 are shown in Figure S5; the assignment of the Sr^{I} and Sr^{II} sites is discussed in the Supporting Information. For SLA, the PLE spectra consist of several overlapping broad bands that are independent of the observation wavelength. By contrast, the PLE measurement of $Sr(LiAl_3)_{1-x}(SiMg_3)_xN_4:Eu^{2+}$ for $x = 0.1$ and 0.5 monitored at 615 and 745 nm, respectively, have a clearly different shape, which suggests the existence of two emission centers denoted as Eu(Sr1) and Eu(Sr2), respectively. For a more detailed consideration of two different centers with $x = 0.1$ and $x = 0.5$, time-resolved luminescence spectra were performed and discussed in the Supporting Information.

To understand the unexpected luminescent properties of SLA-SSM, we sought to understand the practical substitution process during the solid-solution synthesis, which corresponds to determining the occupation value of each ion. Owing to the limitation of the atomic form factor of the X-ray source in distinguishing the occupation value (occ) for Li^+, Mg^{2+}, Al^{3+}, and Si^{4+}, neutron powder diffraction (NPD) is one of the most suitable tools to understand the substitution process in-depth with the aid of joint refinement. The electron numbers for Mg^{2+}, Al^{3+}, and Si^{4+} are the same and they have similar X-ray scattering lengths, while the neutron cross sections are distinct with values of 3.71, 1.503, and 2.167 for Mg^{2+}, Al^{3+}, and Si^{4+}, respectively. Unfortunately, the obtained values of occupation are smaller than or equal to the estimated standard deviation (esd). Without the precise occ value, we tried to investigate indirectly the change of the local size of Sr to understand the change of the crystal field strength of the Eu^{2+} ions. Single-synchrotron refinement provides us an error for Sr–N bond lengths of esd = 0.06 Å. Single-neutron refinement gives and error of esd = 0.035 Å. Joint refinement together decreases the error to esd = 0.02 Å, which reveals the power of joint refinement and the synergy effect. However, in our case, the change of Sr–N bond lengths with the change in concentration x is so subtle that it is not evident because of the complex triclinic crystal structure with six independent Al sites and two Li sites (in total 18 independent atoms, i.e., ≈72 refined parameters). As a result, we cannot obtain reliable information about the change of the crystal field strength of the Eu^{2+} ions through either XRD or NPD and we need to find other ways for further analysis.

Without information about the first coordination shell, the Sr–N bond length, we sought to obtain information on the neighboring cation (tetrahedra) because the volume change of the tetrahedra will also affect the coordination environment of the Sr ions. As a result, the ^{7}Li solid-state nuclear magnetic resonance spectrum (ss-NMR) spectrum was measured (Figure 3). For SLA, two peaks are detected at 2.75 and

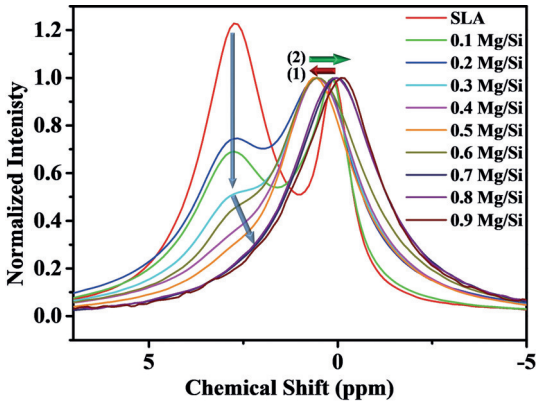

Figure 3. ^{7}Li ss-NMR spectra of $Sr(LiAl_3)_{1-x}(SiMg_3)_xN_4:Eu^{2+}$ with different x values.

0.13 ppm, which correspond to signals from Li1 and Li2, respectively, due to the longer average Li1–N bond length. In contrast, a single peak at −0.08 ppm is obtained for $Sr(LiAl_3)_{0.1}(SiMg_3)_{0.9}N_4:Eu^{2+}$ because there is only one Li site in the SSM structure. According to basic structure information (cif file), the size of the tetrahedron of SSM is smaller than that of SLA, which provides a larger volume for the Sr site in SSM, and a blueshift of the photoluminescence spectrum can be expected. This can also explain why the ss-NMR signal of SSM is at a lower frequency than that of SLA. To compare the results, we normalized the peak of Li2. The peak of Li1 gradually moves toward the upfield region and decreases in intensity, which agrees with our prediction of the gradual shrinking of the $Li(1)N_4$ tetrahedron. The peak of Li2 unexpectedly shifts toward the downfield region peaking at 0.66 ppm for $x = 0.2$–0.6 and shifts toward upfield with the peak maximum at −0.08 ppm for $x = 0.7$–0.9. This result indicates that the $Li(2)N_4$ tetrahedron does not gradually shrink in the same way as $Li(1)N_4$. Instead, the size of the $Li(2)N_4$ tetrahedron first expands and then shrinks. To understand the influence of these interesting results, the environment of Sr1 and Sr2 should be discussed. Sr1 is surrounded by one $Li(1)N_4$ and seven AlN_4 tetrahedra, whereas Sr2 is surrounded by one $Li(1)N_4$, two $Li(2)N_4$, and five AlN_4 tetrahedra. The unexpected behavior of the $Li(2)N_4$ tetrahedra will have a much greater influence on Sr2 than on Sr1. From this point of view, the gradually shrinking of the

$Li(1)N_4$ tetrahedra will cause the gradual expansion of the Sr1 coordination environment, and the blueshift of Eu(Sr1) photoluminescence spectra can be expected. However, the changes in the $Li(2)N_4$ tetrahedra will first shrink the Sr1 coordination environment and then expand it after $x = 0.7$. As a result, the redshift and then blueshift of Eu(Sr2) photoluminescence spectra can be expected.

To test thermal stability, the temperature dependence of the photoluminescence intensity (TDPL) is shown in Figure 4a. According to the TDPL spectra, SLA shows the best thermal stability, which decreases when the Si^{4+} and Mg^{2+} are

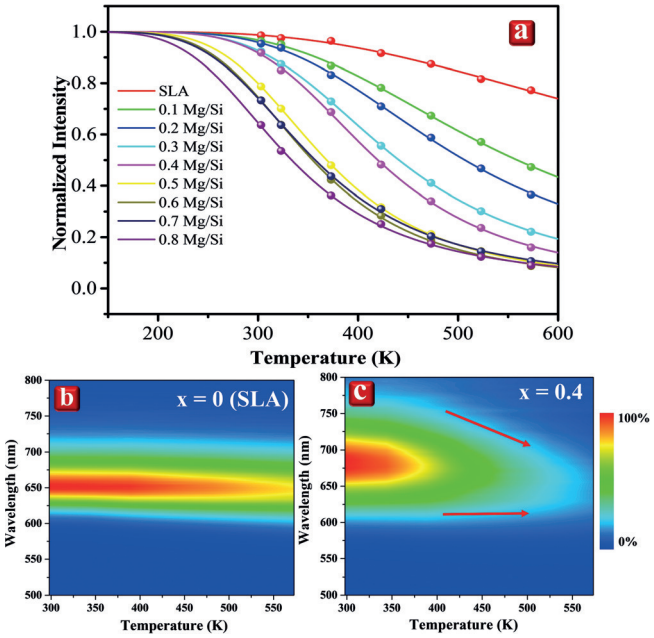

Figure 4. a) TDPL of $Sr(LiAl_3)_{1-x}(SiMg_3)_xN_4:Eu^{2+}$ and the TDPL contour plot of b) SLA and c) $Sr(LiAl_3)_{1-x}(SiMg_3)_xN_4:Eu^{2+}$.

substituted in owing to the decrease of the band gap. According to the literature, the band gaps are around 4.7 and 3.9 eV for SLA and SSM, respectively.[6,7] The decrease of the band gap will easily decrease the difference in energy between the lowest $4f^6 5d^1$ state and the conduction band, and cause thermal ionization, which is the so-called photoionization process, as discussed in the literature.[6] The PL energy difference between SLA and SMS is around 0.1 eV; however, the difference in their band gap energies is around 0.8 eV. Although the energy of the $4f^6 5d^1$ state changes with x in line with the redshift and the blueshift in PL spectra, the decrease of the band gap seems to dominate the thermal quenching process. From the previous study, the HRBE, VRBE, and binding energy are calculated.[19] The results indicate that the position of the Eu^{2+} $5d$ level in SSM is much closer to the conduction band than that of SLA, which results in photoionization and thermal quenching. Furthermore, the energy stabilities for Eu(Sr1) and Eu(Sr2) are different. For SLA, Eu(Sr1) and Eu(Sr2) generate shorter and longer emission wavelengths, respectively, which are extremely close to each other. The TDPL contour plot of SLA is shown in Figure 4b. The emissions from the two Sr sites are hardly distinguishable. The bandwidth and the peak maximum are nearly fixed, which indicates the excellent thermal stability of SLA. However, for $Sr(LiAl_3)_{0.6}(SiMg_3)_{0.4}N_4:Eu^{2+}$, the photoluminescence intensity of the peak maximum decreases much faster than that of SLA when the temperature is increased (Figure 4c). Moreover, the emission from Sr1 is more stable than that from Sr2, as illustrated by the arrow.

Figure S7a and Figure S7b present time-resolved luminescence spectra of $Sr(LiAl_3)_{1-x}(SiMg_3)_xN_4:Eu^{2+}$ at different temperatures for $x = 0.1$ and $x = 0.5$, respectively. At each temperature, the emission is presented for and acquisition time of 0–2 μs time acquisition and for 10 and 500 K and for acquisition times of 0–0.2 and 1–2 μs (dotted curves). The emission spectrum for a timescale of 0–0.2 μs is related to Eu(Sr1) luminescence with a maximum at 650 nm, whereas that for the 1–2 μs timescale is related to Eu(Sr2) luminescence with a maximum at 690 nm. For the timescale 0–2 μs, emission spectra are a superposition of these two: Eu(Sr1) and Eu(Sr2) luminescence but with different contributions for the two samples. In the case of $x = 0.1$, Eu(Sr1) luminescence dominates the emission spectrum unlike at $x = 0.5$, where the Eu(Sr2) luminescence dominates the emission spectrum. With increasing temperature, the $x = 0.1$ emission collected on the timescale of 0–2 μs shifts to lower energies (from 670 nm at 10 K to 650 nm at 500 K); for $x = 0.5$ this decrease is even more significant (from 680 nm at 10 K to 635 nm at 500 K). With an increase of temperature, the intensity of Eu(Sr2) emission decreases strongly for $x = 0.1$ and even more so for $x = 0.5$.

Luminescence decays are obtained by the integration of streak camera images over the wavelength intervals. Decay curves of the 580–620 nm luminescence (which correspond mainly to Eu(Sr2) luminescence) for $x = 0.1$ and $x = 0.5$ are presented in Figure S7c and Figure S7d, respectively. For both samples, these decay curves are non-exponential even at 10 K and become faster with the increase of temperature. Decay curves of the 680–720 nm luminescence (which correspond mainly to Eu(Sr2) emission) for $x = 0.1$ and $x = 0.5$ are presented in Figure S7e and Figure S7f, respectively. Decay curves are single exponential up to 400 K for $x = 0.1$; above this temperature, they become non-exponential and slightly shorten. For $x = 0.5$, decay curves presented in Figure S7f are single exponential up to 200 K and above this temperature they become non-exponential and the decay faster.

After comparing the thermal stabilities, we still sought other more noticeably differences between SLA and SSM and the solid solutions for $x = 0.2$–0.6. We recorded scanning electron microscopy (SEM) images to check the morphology of our samples with the magnitude of 5000. (Figure S8). The morphology of SLA consists of some medium-size particles with some needle structures. The particle size is around 1–5 μm. By contrast, SSM consists of many small particles less than 3 μm in size. However, starting from $x = 0.2$, the particle size noticeably increases. Up to $x = 0.4$, the particle size reaches a maximum with a size of 5–10 μm. This finding indicates that in this range, a new morphology is generated, which is totally different from SLA and SSM.

The X-ray absorption near-edge structure (XANES) spectrum was recorded to define the ratio of Eu^{2+}/Eu^{3+} in

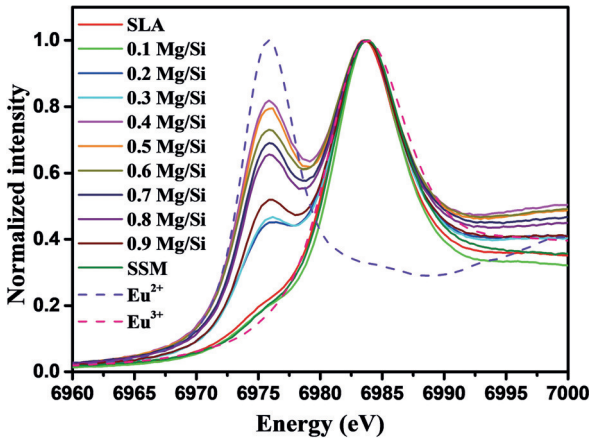

Figure 5. Eu L_3-edge XANES spectra of $Sr(LiAl_3)_{1-x}(SiMg_3)_xN_4:Eu^{2+}$.

the as-prepared samples, which is normalized with Eu^{3+} intensity. (Figure 5). In most of the nitride or oxynitride phosphors, the concentration of Eu^{2+} is much higher than Eu^{3+}. In our experience, the Eu^{2+} concentration in the UCr_4C_4 families will be much lower than the Eu^{3+} concentration.[20] From the XANES spectra, the Eu^{2+} concentration in SLA and SSM is very low. When the Si^{4+} and Mg^{2+} are doped into SLA, the Eu^{2+} relative concentration largely increases and reaches a maximum at $x = 0.4$. To the best of our knowledge, this is the first time that such a high concentration of Eu^{2+} was found in the UCr_4C_4 families. Moreover, for the sample with $x = 0.4$, the XANES spectrum is consistent with the results of SEM and PL spectra. The normalized Eu^{2+} concentration after subtracting the signal from Eu^{3+} is shown in Figure S9. The Eu^{2+} relative concentration in SLA is only approximately 6% of that in the sample with $x = 0.4$, which is a large difference and may cause different performance in photoluminescence intensity. The relative concentration of Eu^{2+} between $x = 0.4$ and SLA changes rapidly; however, the difference in EQE is not very large. This result indicates that the concentration of Eu^{2+} is not the only key point to determine the PL intensity and EQE. The crystal structure and thermal stability must also be considered. However, for one phosphor system, the concentration of the activator, Eu^{2+} in our case, will play an important role in determining the photoluminescence properties. Another interesting fact is that Eu^{2+} ions are larger than Eu^{3+} ions. The noticeable increase of the Eu^{2+} signal may result from the increase in the coordination environment of the Sr1 sites on going from $x =$ 0.2 to 0.6, which is also consistent with our prediction based on ss-NMR spectroscopy.

Integrating the results above, we propose a mechanism of photoluminescence shifting controlled by the size of the coordinated cation (Figure S10). $Sr(LiAl_3)_{1-x}(SiMg_3)_xN_4:Eu^{2+}$ can be divided into two solid-solution systems, from $x = 0$–0.6 and from $x = 0.7$–1.0. In the beginning, the co-doped Mg/Si causes a steady shift of the XRD peak without noticeable phase separation until $x = 0.7$. After $x = 0.7$, the phase transforms from triclinic (SLA) to tetragonal (SSM). We can assume that in the range $x = 0$–0.6, all of the Li is located at its original sites and does not dope in the Al site because only two signals are found in the ss-NMR spectrum. Moreover, during the solid-solution process, $Li(2)N_4$ and $Li(1)N_4$ tetrahedra become larger and smaller, respectively, which will compress the coordination sphere of Sr2 but have much less effect for Sr1. As a result, the unexpected redshift in the photoluminescence spectra is observed. The broadened photoluminescence spectra also prove that the coordination environments of Sr2 and Sr1 become much more different as the Si/Mg dope in. Moreover, the size of the Sr1 site may even exceed our expectation according to the extraordinary high Eu^{2+} signal during this range. After $x = 0.7$, the ^7Li peak is detected, which indicates that the Li may only be located at the Si site in SSM. Finally, from $x = 0.7$–1.0 the structural and photoluminescence properties are similar to those of SSM.

In summary, a series of solid-solution $Sr(LiAl_3)_{1-x}$-$(SiMg_3)_xN_4:Eu^{2+}$ phosphors was successfully synthesized. Synchrotron XRD, neutron diffraction, joint refinement, and Li ss-NMR analysis were performed to further examine the local environment and substitution processes. As the x values increases ($x = 0$–0.6), the expansion of the $Li(2)N_4$ tetrahedra causes the compression of the Sr2 coordination environment. This leads to the stronger crystal field splitting of Eu(Sr2) and the unexpected redshifting in PL from 650–679 nm. On the other hand, the continuous expansion of the volume of Sr2 results in the blueshifting in PL. The broadening of the PL spectrum will enhance the emission area, which also results in higher EQE than SLA. For the first time, a high relative concentration of Eu^{2+} in the XANES spectrum is discovered in a UCr_4C_4-type structure. It can somehow lead to QE higher than that of than SLA itself. The increase in Eu^{2+} concentration may result from the larger Sr1 site during the solid-solution process. SEM analysis also showed that morphology also differs from that of SLA and SSM. Finally, the overall mechanism provides a comprehensive idea during the solid-solution process.

This study can help researchers understand unexpected properties of solid solutions and provide insight in analyzing the local coordination environment for other systems when the substituted ions are complicated.

Acknowledgements

This work was supported by the Ministry of Science and Technology of Taiwan (Contract Nos. MOST 107-2113-M-002-008-MY3 and MOST 107–2923-M-002-004-MY3). This work was supported by the National Science Centre Poland grant Opus no. 2016/23/B/ST3/03911 and the National Centre for Research and Development Poland Grant (No. PL-TW/V/1/2018).

Conflict of interest

The authors declare no conflict of interest.

Keywords: light-emitting diodes · nitride phosphors · solid solutions

How to cite: *Angew. Chem. Int. Ed.* **2019**, *58*, 7767 – 7772
Angew. Chem. **2019**, *131*, 7849 – 7854

[1] Z. Xia, Z. Xu, M. Chen, Q. Liu, *Dalton Trans.* **2016**, *45*, 11214 – 11232.
[2] L. Wang, R. J. Xie, Y. Li, X. Wang, C. G. Ma, D. Luo, T. Takeda, Y. T. Tsai, R. S. Liu, N. Hirosaki, *Light: Sci. Appl.* **2016**, *5*, e16155.
[3] E. F. Schubert, J. K. Kim, *Science* **2005**, *308*, 1274 – 1278.
[4] J. Meyer, F. Tappe, *Adv. Opt. Mater.* **2015**, *3*, 424 – 430.
[5] P. Pust, F. Hintze, C. Hecht, V. Weiler, A. Locher, D. Zitnanska, S. Harm, D. Wiechert, P. J. Schmidt, W. Schnick, *Chem. Mater.* **2014**, *26*, 6113 – 6119.
[6] S. Schmiechen, H. Schneider, P. Wagatha, C. Hecht, P. J. Schmidt, W. Schnick, *Chem. Mater.* **2014**, *26*, 2712 – 2719.
[7] P. Pust, V. Weiler, C. Hecht, A. Tücks, A. S. Wochnik, A.-K. Henß, D. Wiechert, C. Scheu, P. J. Schmidt, W. Schnick, *Nat. Mater.* **2014**, *13*, 891 – 896.
[8] D. Wilhelm, D. Baumann, M. Seibald, K. Wurst, G. Heymann, H. Huppertz, *Chem. Mater.* **2017**, *29*, 1204 – 1209.
[9] P. Strobel, S. Schmiechen, M. Siegert, A. Tücks, P. J. Schmidt, W. Schnick, *Chem. Mater.* **2015**, *27*, 6109 – 6115.
[10] P. Strobel, V. Weiler, C. Hecht, P. J. Schmidt, W. Schnick, *Chem. Mater.* **2017**, *29*, 1377 – 1383.
[11] H. Liao, M. Zhao, M. S. Molokeev, Q. Liu, Z. Xia, *Angew. Chem. Int. Ed.* **2018**, *57*, 11728 – 11731; *Angew. Chem.* **2018**, *130*, 11902 – 11905.
[12] C. Maak, D. Durach, C. Martiny, P. J. Schmidt, W. Schnick, *Chem. Mater.* **2018**, *30*, 3552 – 3558.
[13] M. Zhao, H. Liao, L. Ning, Q. Zhang, Q. Liu, Z. Xia, *Adv. Mater.* **2018**, *30*, 1802489.
[14] P. Strobel, C. Maak, V. Weiler, P. J. Schmidt, W. Schnick, *Angew. Chem. Int. Ed.* **2018**, *57*, 8739 – 8743; *Angew. Chem.* **2018**, *130*, 8875 – 8879.
[15] J. L. Leaño, M. H. Fang, R. S. Liu, *ECS J. Solid State Sci. Technol.* **2018**, *7*, R3111 – R3133.
[16] S. Kim, T. Hasegawa, S. Hasegawa, R. Yamanashi, H. Nakagawa, K. Toda, T. Ishigaki, K. Uematsu, M. Sato, *RSC Adv.* **2016**, *6*, 61906 – 61908.
[17] D. Cui, Q. Xiang, Z. Song, Z. Xia, Q. Liu, *J. Mater. Chem. C* **2016**, *4*, 7332 – 7338.
[18] M. H. Fang, W. L. Wu, Y. Jin, T. Lesniewski, S. Mahlik, M. Grinberg, M. G. Brik, A. M. Srivastava, C. Y. Chiang, W. Zhou, D. Jeong, S. H. Kim, G. Leniec, S. M. Kaczmarek, H. S. Sheu, R. S. Liu, *Angew. Chem. Int. Ed.* **2018**, *57*, 1797 – 1801; *Angew. Chem.* **2018**, *130*, 1815 – 1819.
[19] D. Cui, Z. Song, Z. Xia, Q. Liu, *Inorg. Chem.* **2017**, *56*, 11837 – 11844.
[20] M. H. Fang, Y. T. Tsai, H. S. Sheu, J. F. Lee, R. S. Liu, *J. Mater. Chem. C* **2018**, *6*, 10174.

Manuscript received: March 14, 2019
Accepted manuscript online: April 8, 2019
Version of record online: April 29, 2019

